Spatial Phase Synchronisation of Pistachio Alternate Bearing: Common-Noise-Induced Synchronisation of Coupled Chaotic Oscillators

Kenshi Sakai[a,*], Patrick Brown[b], Todd Rosenstock[c], Shrini Upadhyaya[d], Alan Hastings[e,f]

[a]Department of Environmental and Agricultural Engineering, Tokyo University of Agriculture and Technology, Fuchu, Tokyo 183-8509, Japan.

[b]Department of Plant Science, University of California, Davis, CA 95616, USA.

[c]Land Health Decisions, World Agroforestry (ICRAF), 13 Avenue des Cliniques, Kinshasa, Democratic Republic of Congo.

[d]Department of Biological and Agricultural Engineering, University of California, Davis, CA 95616, USA.

[e]Department of Environmental Science & Policy, University of California, Davis, CA 95616, USA.

[f]Santa Fe Institute,1399 Hyde Park Rd., Santa Fe, NM 87501, USA.

***Correspondence to Kenshi Sakai.**

Email: ken@cc.tuat.ac.jp

Abstract

The collective dynamics of chaotic oscillators has drawn considerable attention in numerous fields, including agriculture and forestry. The alternate bearing of tree crops is a phenomenon in which a year of heavy yield is followed by a year of light yield. This phenomenon has been conventionally investigated using a tent map known as a resource budget model. Alternate fruiting is caused by strong synchronisation among trees in an orchard and is a major problem in fruit growing. To develop control methods for alternate fruiting, it is essential to understand the strength of synchronisation at the individual and population levels of trees in orchards and the mechanism of alternate fruiting. In this study, in-phase/out-of-phase analysis was applied to the yield data of a 9,562 pistachio (*Pistacia vera* L.) population, and the phase transitions and mode-locking in the orchard were revealed. Using a developed network model consisting of diffusively coupled chaotic oscillators on which common noise was imposed identically, the phase transitions, mode-locking, and 1/3 power-law scaling spatial correlation were confirmed mathematically. Furthermore, the manner in which three essential factors, i.e. common noise, direct coupling, and the cropping coefficient gradient, explain the spatial synchrony of the orchard was elucidated. The proposed methodology based on nonlinear dynamics would be useful for pomology, forestry, and ecosystem management.

Keywords: Common-noise-induced synchronisation, Coupled networks, Alternate bearing, *Pistacia vera* L., Chaotic oscillators

1. INTRODUCTION

Alternate bearing (biennial bearing) is a common synchronisation in several tree crops in which a year of heavy yield (on-year state) is followed by a year of light yield (off-year state). Citrus fruits (e.g. oranges, lemons, and mandarins) and nuts (e.g. pistachios, pecan, and walnuts) are typical alternate-bearing crops [1–9] that generally show a dominant two-year cycle (i.e. period-two) synchronisation. Masting is also a synchronisation among tree species in which there are multiple- and mixed-year cycles [10–14]. Such a large on-off two-year cycle of crop production negatively affects profitability and resource (i.e. water, nutrient, and labour) efficiency. Measuring the strength of the spatial synchrony in both individual trees and populations is useful for obtaining knowledge to suppress and/or predict alternate bearing.

Using the in-phase/out-of-phase analysis technique, we determined the strength of the phase synchronisation in 9,562 individual trees over six years. We identified three unique features of alternate bearing in the orchard: the phase transition, mode-locking, and 1/3 power-law scaling spatial correlations.

To explain the three features, we developed a model of alternate bearing based on switching dynamics using the resource budget model (RBM) [15] of perennial plant species [7–9, 12–18]. The pollen limitation theory has been established for cross-pollinating species to model their alternate bearing and/or masting. They are formulated using global coupling maps [12–15] and local coupling maps [19–20] with mean-field pollen coupling. However, the pollen limitation theory cannot be applied to dioecious plant species such as pistachio because male trees consistently supply sufficient pollen to female trees every year. Instead, the concept of common noise-induced synchronisation was introduced to explain the alternate bearing of pistachio trees [7–9, 21]. These models are all prevalent in nonlinear physics [22–26]. Common noise

synchronisation is a phenomenon in which a nonlinear (even chaotic) oscillator population is synchronised when an irregularly fluctuating external force acts identically on all the oscillators.

Based on the observed spatial correlation with 1/3 power-law scaling, we assumed the existence of direct coupling considering an underground root grafting and mycorrhizal network [1, 27–34] and incorporated the diffuse coupling term into the development model in a formula that enhances phase synchronisation.

Applying the in-phase/out-of-phase method to yield data and numerical experiments, we confirmed that common noise, spatial gradients of crop coefficients, and diffusive direct coupling are three essential factors in explaining phase transitions, mode-locking, and 1/3 power-law scaling spatial corrections.

2. EXPERIMENTAL INVESTIGATIONS

2.1 Alternate bearing and spatial correlation of the yield data

The number of pistachio trees in the orchard (N) = 9,562; the male pistachio (*Pistacia vera* L.) trees were evenly spaced (26 m × 26 m); female trees were located within 14 m of the nearest male trees to receive sufficient pollen. The data were obtained from a 32.3 ha (416 m × 777 m) orchard located at 35° 86′ N, 119° 87′ W (Lost Hills, Kings County, California, USA) [7–9]. The trees were spaced 5.2 m and 6.4 m apart in rows and columns, respectively (Fig. 1a).

Alternate bearing is a phenomenon in which a heavy harvest (*ON*-year) and a light harvest (OFF-year) repeat almost two years in many tree crops. The states of 'ON-year' and 'OFF-year' of a population were determined as follows [17]. Let $x_i(t)$ be the yield of tree i at time t (year). The phase angle of $x_i(t)$ is given by $\theta_i(t) =$

93 angle$(HT[x_i(t) - \bar{x_i}])$, where *HT* is the Hilbert transform, and $\bar{x_i}$ is the time average
94 of $x_i(t)$. For *ON*-year and *OFF*-year, $\frac{1}{N}\sum_{i=1}^{N}\cos\theta_i(t) > 0$ and $\frac{1}{N}\sum_{i=1}^{N}\cos\theta_i(t) \leq 0$,
95 respectively. As shown in Fig. 1b, ON-year and OFF-year repeated in a two-year cycle,
96 except for 2002 and 2003, in which ON-year occurred in succession. The production in
97 2003 was between that of ON-year and OFF-year; the west side production was
98 significant, but the east side production was marginal. However, by the definition of
99 ON-year state and OFF-year state, 2003 was classified as ON-year [16, 17]. In 2004, the
100 production of the west area was extremely low, and that of the east side was marginally
101 higher. Although this trend is qualitatively opposite to that in 2003, as the total
102 production was significantly lower than the annual average yield of the orchard, 2004
103 was an OFF-year. In 2005, high yields were obtained throughout the orchard; however,
104 meagre yields were followed in 2006.
105 The yield of the majority of trees exhibited a two-year cycle oscillation. At the
106 same time, the population also showed two-year periodic fluctuations due to
107 synchronisation among trees. Thus, the yield data represent a typical case of alternate
108 bearing.

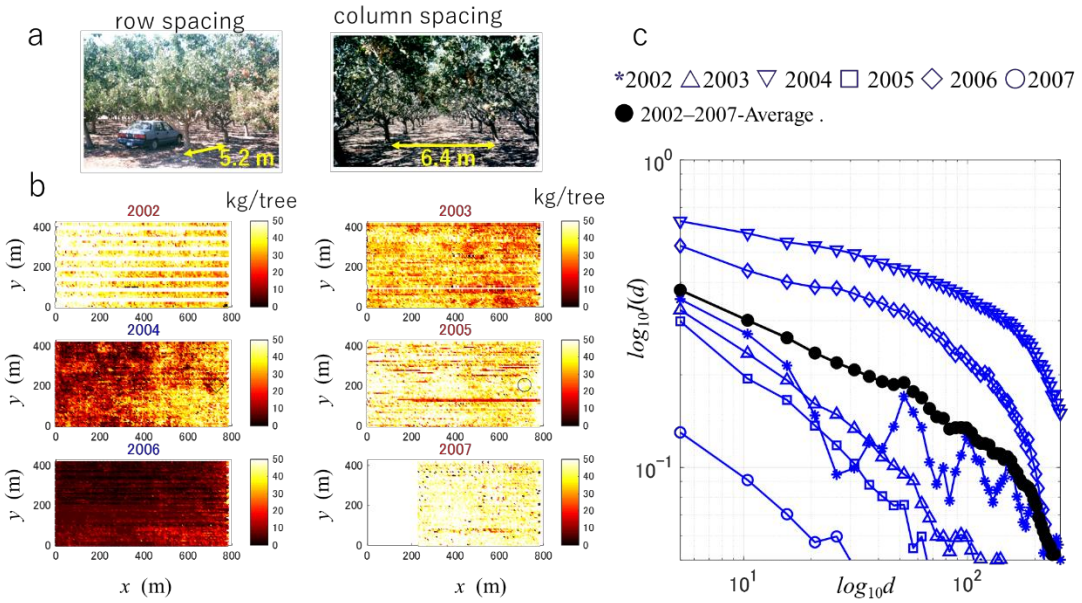

Fig. 1. Spatial correlations of the yield of the orchard for 2002–2007.
(a) Column spacing and row spacing of the orchard.
(b) Yield maps for 2002–2007.
(c) Moran's I; *I*(d) for six years and the averaged *I*(d):
* 2002, △2003,▽2004, □2005,◇2006, ○2007, ● 2002–2007 (average).
The area of the orchard was 32.3 ha (416 m × 777 m) during 2002–2006. In 2007, the trees in the western part of the orchard were removed; hence the area of the orchard was 22.7 ha [18].

Fig. 1c shows the spatial correlations of the yields corresponding to Fig. 1b. The spatial correlation coefficient *I*(d), known as Moran's I, is commonly used in ecology [19,35] and defined by Eq. (1).

$$I(d) = \frac{N}{W}\frac{\sum_{i=1}^{N}\sum_{j=1}^{N} w(i,j)[x_i(t)-\bar{x}(t)][x_j(t)-\bar{x}(t)]}{\sum_{i}^{N}[x_i(t)-\bar{x}(t)]^2}, \quad (1)$$

where N denotes the number of spatial units indexed by i and j; $x_i(t)$ is the yield, $\bar{x}(t)$ is the mean of $x_i(t)$, and $w(i,j)$ is a matrix of spatial weights with zeros on the diagonal ($i = 1,\ldots, N$; $w(i, i) = 0$). Here, W is the sum of all $w(i,j)$.

$$w(i,k) = \begin{cases} 1 & |D(i,j) - r| \le \Delta d \\ 0 & |D(i,j) - r| > \Delta d \end{cases}, \quad (2)$$

where $D(i,k)$ denotes the distance between trees i and k.

The short-range correlation coefficients at 5.2 m in 2004 and 2006 were as high as 0.63 and 0.53, respectively, while the long-range correlation remained relatively high. In 2002, 2003, and 2007, the short-range correlation coefficients were 0.35, 0.33 and 0.30, respectively. In 2006, the spatial correlation was significantly lower at 0.13. The six-year average of $I(d)$ is represented by solid black circles, indicating 1/3 power-law scaling spatial correlation. Thus, three characteristics of the spatial correlation were observed in the orchard: (i) high short-range spatial correlation, (ii) long-range spatial correlation with 1/3 power-law scaling, and (iii) wide range variation of $I(d)$ on the time (year) domain.

2.2 Phase synchronisations detected in the orchard

***2.2.1.* Measures of phase synchrony:** The phase synchronisation of a population comprises two classes: in-phase and out-of-phase. Let $x_i(t)$ be the yield of the i^{th} tree in year t and $\emptyset(\mathrm{i},\mathrm{j},t)$ be the phase between the i^{th} and j^{th} trees, then

$$\emptyset(i,j,t) = \{x_i(t+1) - x_i(t)\}\{x_j(t+1) - x_j(t)\}. \quad (3)$$

The fraction of the in-phase behaviour of tree i relative to the remaining trees in the population (size N) in year t is defined as

$$f_{in}^{i}(t) = \frac{1}{N-1}\sum_{j=1,j\neq i}^{N} H\big(\emptyset(i,j,t)\big), \quad (4)$$

where H is the Heaviside step function.

The fraction with in-phase behaviour $F_{IN}(t)$ within a population (size N) for year t is given by

$$F_{IN}(t) = \sum_{i=1}^{N} f_{in}^{i}(t), \quad (5)$$

where $f_{in}^{i}(t)$ and $F_{\mathrm{IN}}(t)$ quantify the strength of in-phase synchronisation for the individual tree and population, respectively. $F_{IN}^{K}(t)$ (K = 1, 2, ... , 30) denotes the west–east spatial average of $f_{in}^{i}(t)$ for every five columns. $\bar{F}_{IN}^{K}$ and $\bar{f}_{in}^{i}$ are the time (year) averages of $F_{IN}^{K}(t)$ and $f_{in}^{i}(t)$.

$\bar{F}_{IN}^{K}$ = 1 and $\bar{f}_{in}^{i}$ = 1 indicate all trees behaving in the same state (ON-year or OFF-year states). In other words, $\bar{F}_{IN}^{K}$ = 1 and $\bar{f}_{in}^{i}$ = 1 indicate the presence of perfect in-phase synchronisation, representing 'order' in a population. In the case of a population of sufficiently large size, $\bar{F}_{IN}^{K}$ = 0.5 and $\bar{f}_{in}^{i}$ = 0.5 indicate all trees behaving randomly and represent 'disorder'. Note that the value of $\bar{F}_{IN}^{K}$ and $\bar{f}_{in}^{i}$ is in the range of [0.5, 1.0].

2.3.2 Phase transitions and mode-locking in the orchard: Using the defined measures, we reveal the unique features of phase synchronisation observed in the orchard. Figs. 2(a) –(e) demonstrate the time evolution of the spatial distribution of phase synchronisation in the five periods of two successive years: [2002–2003], [2003–2004], [2004–2005], [2005–2006], and [2006–2007] in five rows, respectively. The orchard was divided into 14 blocks by rows and columns: (rows × columns) = (2 × 7). The value of $f_{in}^{i}(t)$ was calculated for each tree *i* within the block to which tree *i* belonged. The first and second column panels show the spatial distributions of $f_{in}^{i}(t)$ and $F_{IN}^{K}(t)$, respectively, vs *K*.

The strength of phase synchronisation in the period [2002–2003] was weaker than in other periods, as shown in Figs. 2a(i) and (ii). In the following periods, [2003–2004] and [2004–2005], the strength of phase synchronisation increased, and the spatial

distribution of phase synchronisation from west to east became distinct, i.e. stronger in the west and weaker in the east. $F_{IN}^{1}(2004)$ and $F_{IN}^{30}(2004)$ were 0.98 and 0.56, respectively, indicating perfect phase synchronisation in the west and perfect phase desynchronisation in the east. These spatial phase transitions from west to east are attributes of this orchard.

In the periods [2005–2006] and [2006–2007], perfect phase synchronisation dominated, with $f_{in}^{i}(2006)$ and $f_{in}^{i}(2007)$ reaching 1.0 for the whole orchard and $F_{IN}^{K}(2005)$ and $F_{IN}^{K}(2006)$ almost 1.0 for any *K*. The fact that the perfect synchronisation mode lasted in two periods, [2005–2006] and [2006–2007], gives experimental evidence that mode-locking can occur even in real orchards.

Fig. 2f shows the time-averaged spatial phase transition for the above five periods. As shown in the $\bar{f}_{in}^{i}$ map in Fig. 2f(i), $\bar{f}_{in}^{i}$ was almost 1.0 for several trees in the western block and almost 0.5 for a few trees in the eastern block. $\bar{F}_{IN}^{K}$ decreased from 0.92 to 0.7 from west to east (Fig. 2f(ii)). These results indicate that the strength of the phase synchronisation significantly declined from west to east. In this orchard, alternate bearing was severe in the west and moderate in the east. Mitigating alternate bearing is a critical issue for fruit production. Therefore, we focused on elucidating the mechanism of the east–west directional phase transition.

Here, we demonstrate that the phase transitions emerge both spatially and temporally in the orchard. The measures such as $f_{in}^{i}(t), \bar{f}_{in}^{i}, F_{IN}^{K}(t)$, and $\bar{F}_{IN}^{K}$ successfully provide detailed information on the spatial and temporal behaviour of the features of phase synchronisations.

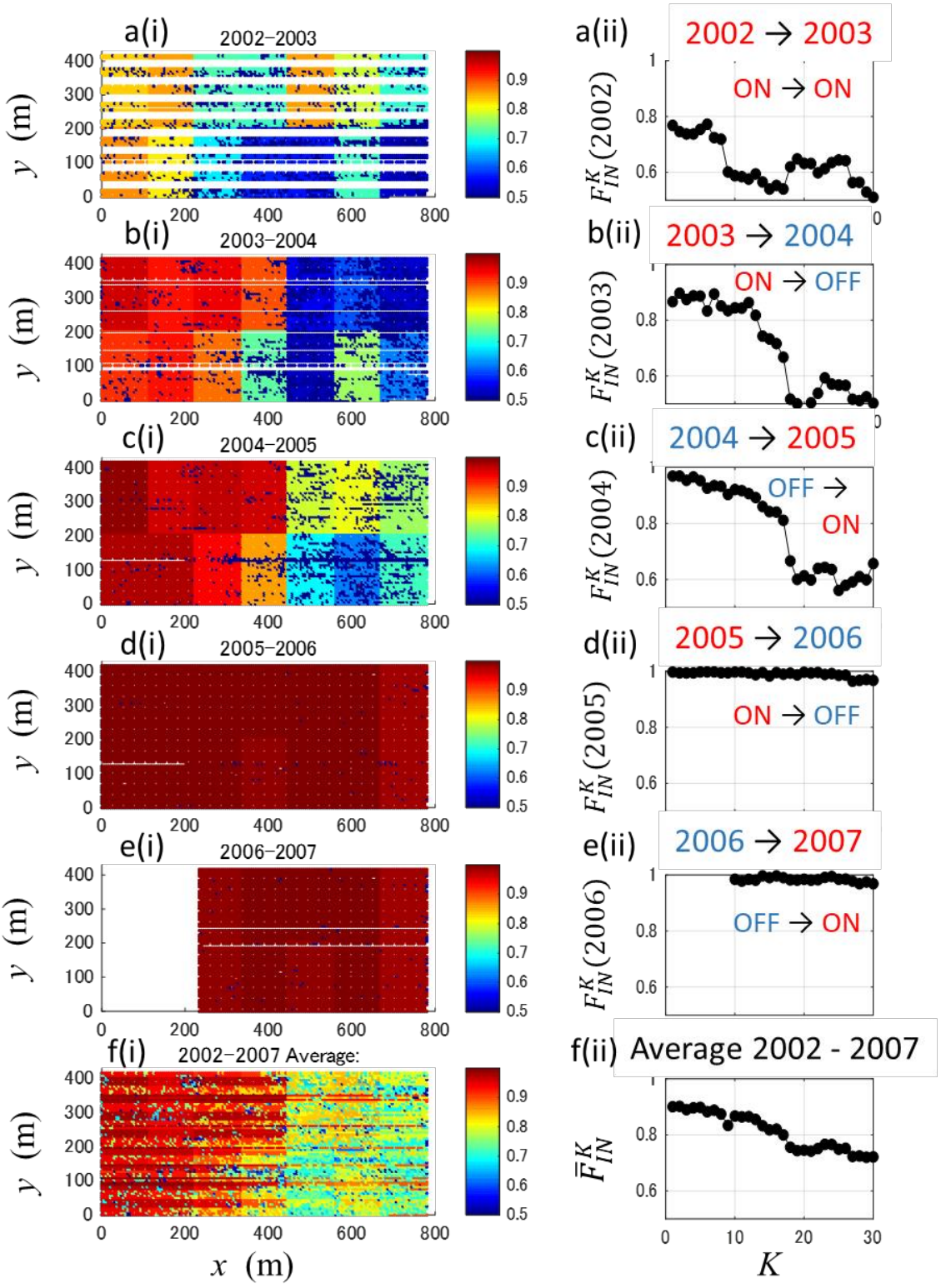
a(i)
2002–2003
b(i)
2003–2004
c(i)
2004–2005
d(i)
2005–2006
e(i)
2006–2007
f(i)
2002–2007 Average:
y (m)
x (m)
a(ii)
2002 → 2003
ON → ON
b(ii)
2003 → 2004
ON → OFF
c(ii)
2004 → 2005
OFF → ON
d(ii)
2005 → 2006
ON → OFF
e(ii)
2006 → 2007
OFF → ON
f(ii) Average 2002 - 2007
K

197

Fig. 2. Time evolution of the spatial phase transitions in the orchard;
a(i)–e(i) 2D spatial distribution of phase synchronisation: $f_{IN}^{i}(t)$ maps for 2002–2003; 2003–2004, 2004–2005, 2005–2006, and 2006–2007;
a(ii)–e(ii) $F_{IN}^{K}(t)$ vs K plots for 2002–2003, 2003–2004, 2004–2005, 2005–2006, and 2006–2007 periods in the orchard;
f(i) shows $\bar{f}_{in}^{i}$ map for 2002–2007 (average); f(ii) shows $\bar{F}_{IN}^{K}$ vs K for 2002–2007 (average).

3. MODEL DEVELOPMENT

3.1 Network dynamics with identically imposed common noise

Strong synchronisation, spatial and temporal phase transitions, and 1/3 power-law scaling spatial correlation are three features of the yield data, as shown in Fig. 1 and Fig. 2. To identify the possible mechanism that generates the three features, we developed a model consisting of a diffusively coupled network of chaotic oscillators with a common noise imposed on them identically.

3.1.1 Chaotic Oscillator: The RBM is a tent map used for modelling the switching dynamics of the fruiting process of perennial plants (Fig. 3a). $S^{i}(t)$ represents the amount of resource reserves at the beginning of year t for three is, P_S is the annual resource input (e.g. photosynthetic residue [15] or unspecified substances [36, 37]) accumulated by the next flowering season in the trunk of a plant, and L_t is the capacity of the trunk.

If the accumulated resource $S^{i}(t) + P_S$ exceeds the capacity (L_t), the excess $S^{i}(t) + P_S - L_T$ is used for the flowering cost $C_f^{i}(t)$; otherwise, $C_f^{i}(t) = 0$ indicating no flowering.

$$C_f^{i}(t) = \begin{cases} S^{i}(t) + P_S - L_T & S^{i}(t) + P_S > L_T \\ 0 & S^{i}(t) + P_S \leq L_T \end{cases} \quad (6)$$

The fruiting cost is

$$C_a^i(t) = m_i C_f^i(t), \tag{7}$$

where the cropping coefficient m_i is defined as the product of the cost ratio $R_C = C_a^i(t)/C_f^i(t)$ and the fruiting coefficient Z.

$$m_i = R_C Z_i \tag{8}$$

$S^i(t+1)$ is given by

$$S^i(t+1) = S^i(t) + P_S - C_f^i(t) - C_a^i(t). \tag{9}$$

The map $S^i(t) \to S^i(t+1)$ is Isagi's RBM [15], popularly known in population ecology. Fig. 3b is the return plot given by Eq. (9); thus, the RBM is a roof-top tent map. For $m = 1.4$, the fixed point $S^* = L_T - \frac{R_C}{1+R_C} P_S$ is unstable. Interestingly, the stitching circuits of a current-mode-controlled boost converter also have the same dynamics [38, 39] as RBM, which has two-band chaos with a critical bifurcation (Fig. 3c).

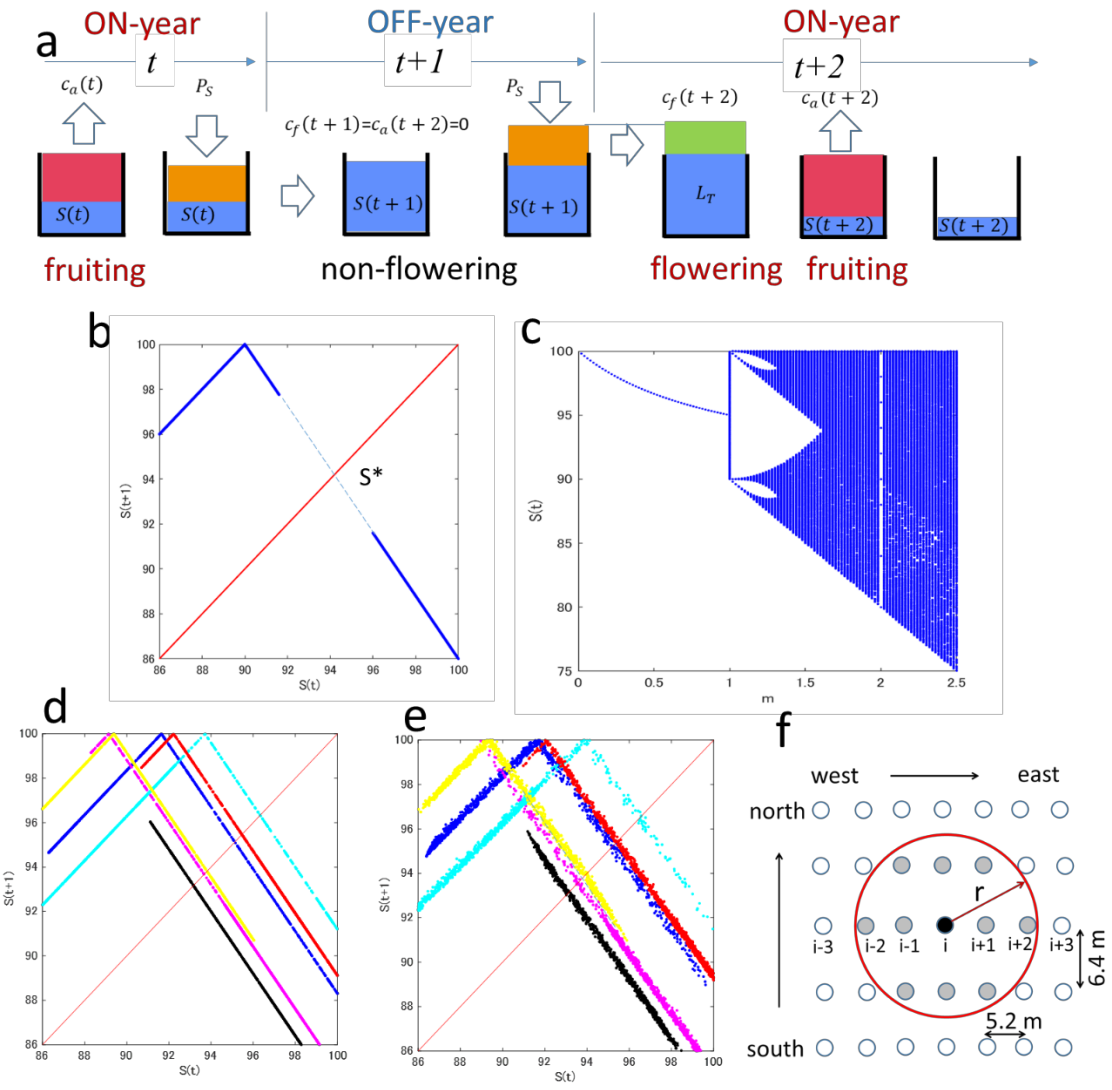

Fig. 3. Switching dynamics of resource budget model (RBM).
(a) Schematic diagram of the process of generating alternate bearing described by Eqs. (6)–(9); m = 1.4, and the unstable fix point $S^* = L_T - \frac{R_C}{1+R_C}P_S$.
(b) Return plot generated by RBM switching dynamics of Eq. (9). After 1000 iterations, the last 100 years for 1000 individual trees are plotted.
(c) Bifurcation diagram of RBM.
(d) Return plot generated by Eq. (9) and common noise (Eq. (12)). After 1000 iterations, t = 994–1000 of the last seven years for 1000 individuals are plotted using blue, magenta, cyan, black, yellow, and red.
(e) Return map generated from the RBM networks dynamics incorporating diffusive coupling using Eq. (14). After 1000 iterations, t = 994–1000 of the last seven years for 1000 individuals are plotted using blue, magenta, cyan, black, yellow, and red.
(f) Arrangement of trees in the network model. The diffusive coupling occurs between individual trees within a distance r from tree i.

3.1.2 m-gradient: As shown in Fig. 1, the strength of phase synchronisation decreased from west to east. By formulating Eqs. (10) and (11), Z_i and m_i vary from 1 to R_C from west to east in the orchard.

$$Z_i = \frac{1}{R_C} + (1 - \frac{1}{R_C}) \frac{x_i}{L_{WE}}, \tag{10}$$

$$m_i = 1 + \alpha \frac{x_i}{L_{WE}}, \tag{11}$$

where (x_i, y_i) are the spatial coordinates of the i^{th} tree. L_{WE} is the distance from the west end to the east end. $L_{WE} = 780\ m$. The spatial slope of the cropping coefficient m_i is set to $\alpha = R_C - 1$ for m_i to increase linearly from 1 to R_C from west to east of the orchard.

3.1.3 Common noise e_C: This study assumes that the synchronisation of the pistachio (*Pistacia vera* L.) population is common-noise-induced. The common noise *CE*(t), presuming an external environmental force, is imposed on all trees identically.

$$CE(t) = e_C \sigma(t), \tag{12}$$

$$P_S(t) = P_0\{1 + CE(t)\}, \tag{13}$$

where P_0 denotes the intrinsic annual surplus, and $\sigma(t)$ is the normal distribution $N(\mu, \sigma^2) = N(0,1)$. The level of common noise is represented by e_C.

Replacing P_S in Eq. (9) by $P_S(t)$, we have the map $S^i(t+1) \rightarrow S^i(t)$:

$$S^i(t+1) = S^i(t) + P_S(t) - C_f^i(t) - C_a^i(t). \tag{14}$$

Since the common noise *CE*(t) is imposed on all trees identically, the tent map given by Eq. (14) does not change its roof-top shape but translates horizontally according to *CE*(t) (Fig. 3d).

3.1.4. Diffusive coupling ε: We assumed the existence of a root system network that allowed material exchange between trees [27–29] and implemented the coupling in the form

$$SA^i(t) = S^i(t) + \frac{1}{M(i)} \sum^{N}_{\substack{i \neq j \\ d(i,j)<r}} \varepsilon_{j,i}\left[S^j(t) - S^i(t)\right], \tag{15}$$

where $\varepsilon_{j,i}$ is the diffusive coupling term, $d(i,j)$ is the distance between tree *i* and tree *j*, and $M(i)$ is the number of trees located within the coupling range *r* (m) from tree *i*, (see Fig. 3f). $SA^i(t)$ is the amount of resource when material exchanges before flowering.

$$C_f^i(t) = \begin{cases} SA^i(t) + P_S(t) - L_T & SA^i(t) + P_S(t) > L_T \\ 0 & SA^i(t) + P_S(t) \leq L_T \end{cases} \tag{16}$$

$C_a^i(t)$ is determined in Eq. (7).

Thus, the map of the developed model $S(t) \rightarrow S(t+1)$ is

$$S^i(t+1) = SA^i(t) + P_S(t) - C_f^i(t) - C_a^i(t) \tag{17}$$

Fig. 3e is the tent map given by Eq. (17). The minor disturbances on the maps are due to the diffusive coupling ε and not stochastic noise.

4. NUMERICAL EXPERIMENTS

4.1 Effect of essential parameters

To quantify the effects of the three parameters on specific features such as strong in-phase synchronisation, spatial and temporal phase transitions, and spatial correlation of 1/3 power-law scaling, numerical experiments were performed for four different combinations of the three parameters (e_C, ε, α), and the results are shown in Fig. 4. The coupling range was r = 11 m (Fig. 3f) in the numerical experiments.

Given the combinations of the three parameters (e_C, ε, α), the best fit common noise (external force) *CE*(t) was determined as follows. The initial values of $S^i(1)$ for 9,562 trees were given as uniform random numbers in (L_T-P_0, L_T), and the common noise *CE*(t) was given as a normal random number for *t* (Eq. (12)). The model was run until *t* reached 5000, and the best fitting 25 years period with respect to $\bar{F}_{\mathrm{I}\mathbb{N}}^{K}$ was selected. With the *CE*(t) of the selected 25 years, $\bar{F}_{\mathrm{I}\mathbb{N}}^{K}$ vs K plots, $\bar{f}_{\mathrm{in}}^{\mathrm{i}}$ maps, and *I*(d) diagrams are displayed in panels (i), (ii), and (iii), respectively, for each combination of (a)–(d) (Fig. 4).

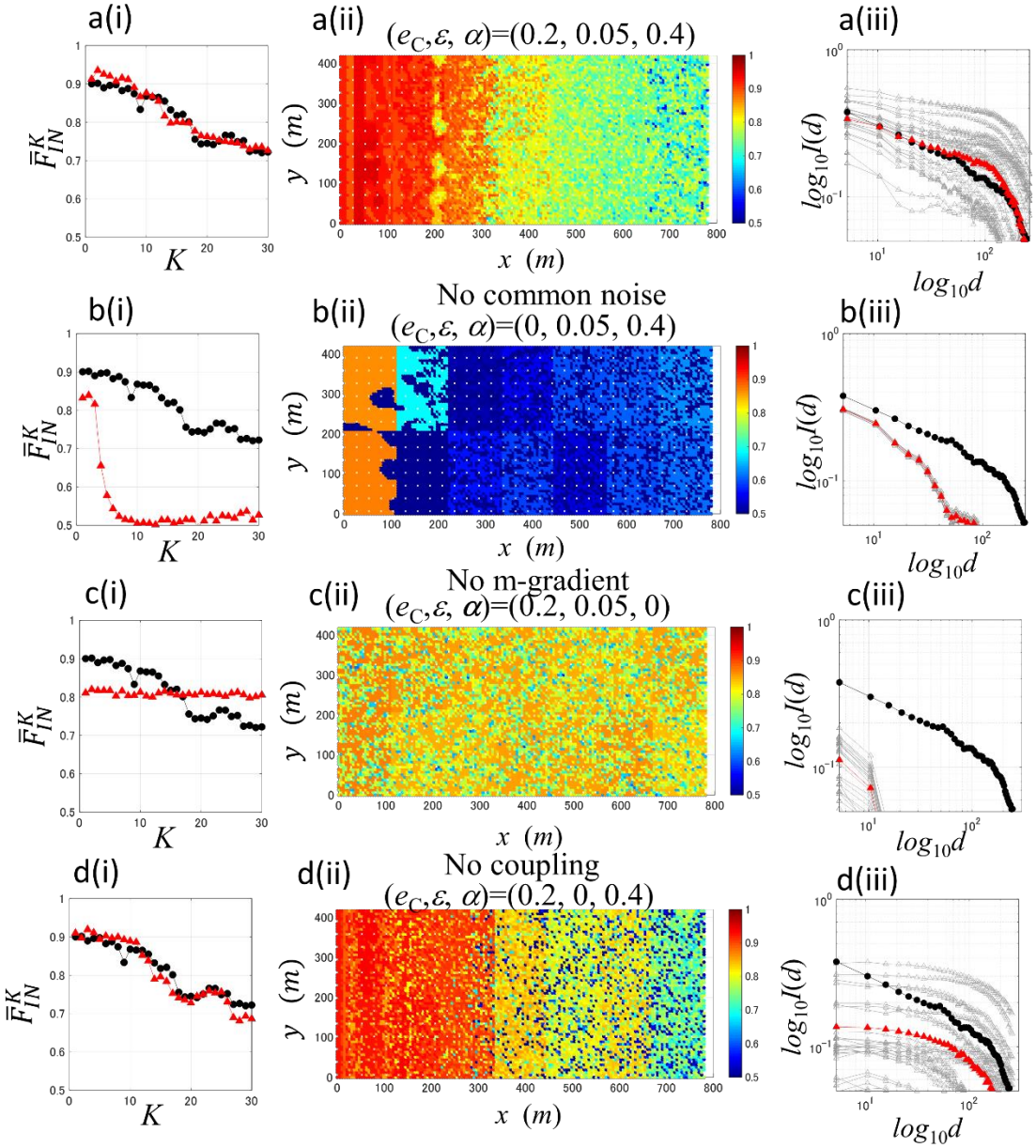

Fig. 4. Effects of each of three essential parameters on spatial phase transitions and spatial correlations; common noise (e_C), diffusive coupling (ε), and m-gradient (α).
(a) With three essential factors; (e_C, ε, α) = (0.05, 0.2, 0.4), and R_C=1.4.
(b) No common noise; (e_C, ε, α) = (0.05, 0, 0.4), and R_C=1.4.
(c) No diffusive coupling; (e_C, ε, α) = (0.05, 0, 0.4), and R_C=1.2.
(d) No m-gradient; (e_C, ε, α) = (0.05, 0,2, 0), and R_C=1.4.

Fig. 4a shows the case where the all three parameters are present, with (e_C, ε, α) = (0.2, 0.05, 0.4). The actual and model plots of $\bar{F}_{IN}^K$ (Fig. 4a(i)) and the map of $\bar{f}_{\text{in}}^{\text{i}}$ (Fig. 3a(ii)) are consistent with the real data shown in Fig. 1f. Fig. 4a(iii) shows that the

spatial correlation I(d) satisfied the following three properties. First, the two highest I(d) were 0.55 and 0.51 at d = 5.2 m, indicating a high short-range spatial correlation. Second, even at d =100 m, I(d) was greater than 0.38, indicating that long-range spatial correlation accompanies 1/3 power-law scaling. Third, I(d) varied widely over the same range as the real data (see Fig. 1(c)).

To confirm the effect of the common noise, the case with no common noise (e_C, ε, α) = (0, 0.05, 0.4) is examined in Fig. 4b. On the west edge (K=1–3), $\bar{F}_{IN}^{K}$ was higher than 0.8, indicating moderate phase synchronisation, and with an increase in K, $\bar{F}_{IN}^{K}$ rapidly decreased to 0.5, indicating no in-phase synchronisation (Figs. 4b(i) and (ii)). As shown in Fig. 4b(iii), I(d) had a moderate short-range spatial correlation, with I(d) = 0.31 at d = 5.2 m; however, there was no significant long-range spatial correlation, no evident power-row scaling, and no yearly variation in $I(d)$. The results suggest that common noise is indispensably essential in explaining the synchronisation observed in the orchard. This result supports the hypothesis that the synchronisation of dioecious plant species such as pistachio is 'common-noise-induced synchrony'.

The role of m-gradient is demonstrated in Fig. 4c. In this case, (e_C, ε, α) = (0.2, 0.05, 0); according to Eq. (11), m = 1.2 everywhere in the orchard. Figs. 4c(i) and (ii) show that $\bar{F}_{IN}^{K}$ and $\bar{f}_{\mathrm{in}}^{\mathrm{i}}$ were approximately 0.8, indicating the presence of alternate bearing as a phase synchronisation. However, no spatial phase transitions are seen in Figs. 4c(i) and (ii). These results suggest that even with the presence of both common noise (e_C) and coupling (ε), the gradient of m is needed for explaining the spatial correlations and spatial phase transition, as observed in Fig. 2.

Fig. 4d shows the case without coupling (e_C, ε, α) = (0,2, 0, 0.4). The $\bar{F}_{IN}^{K}$ plot (Fig. 4d(i)) and the map of $\bar{f}_{\mathrm{in}}^{\mathrm{i}}$ (Fig. 4d(ii)) show that the strength of phase synchronisation declined from west to east. In terms of spatial phase transition, this case showed good agreement with the real data. However, Fig. 4d(iii) indicates that the short-range spatial correlations were significantly smaller than those of the real data (Fig. 1c), and power-law scaling did not exist, although year-to-year variations were observed. This result suggests that diffusive coupling is necessary to realise all three features of phase synchronisations observed in the orchard.

4.2 Spatio-temporal behaviour of phase synchronisations

Numerical experiments shown in Fig. 5 demonstrate that common noise, direct coupling, and *m*-gradient were necessary to realise features such as strong phase synchronisation (alternate bearing), spatial and temporal phase transitions, and 1/3 power-law scaling of spatial correlation in the orchard.

The phase transitions in both the spatial and temporal domains constitute the nature of the dynamics observed in the orchard substantially, as described in Fig. 2. To examine the phase transitions in the time (annual) domain, the 24 panels shown in Fig. 5 include $F_{IN}^{K}(\mathrm{t})$ vs K plots of 24 periods from 25 years. The perfect in-phase synchronisations occurred when t = 1, 2, 3, 22, and 23 (highlighted in yellow). Three consecutive periods (t = 1, 2, and 3) and two consecutive periods (t = 22 and 23) indicated mode-locking. In both field experiments (Fig. 1) and numerical experiments (Fig. 5), mode-locking occurred only in the alternate states, i.e. 'ON→OFF' or 'OFF→ON' periods.

The distinct west-to-east phase transitions occurred at t = 4, 5, 6, 11, and 12 in the alternate states (highlighted in magenta). In the west half of the orchard, $F_{\mathrm{I}\mathbb{N}}^{K}$

remained at approximately 1.0, indicating strong in-phase synchronisation; however, the value sharply decreased to approximately 0.5, indicating desynchronisation in the east half. Conversely, weaker phase synchronisations occurred in non-alternate states, i.e. 'ON→ON' or 'OFF→OFF' periods. The former case observed in the orchard is shown in Fig. 2a (in 2002), and the latter case is shown in Fig. 5 at t = 20 (highlighted in blue). Thus, the numerical experiments reproduced various patterns of spatio-temporal phase transitions obtained from the experimental data.

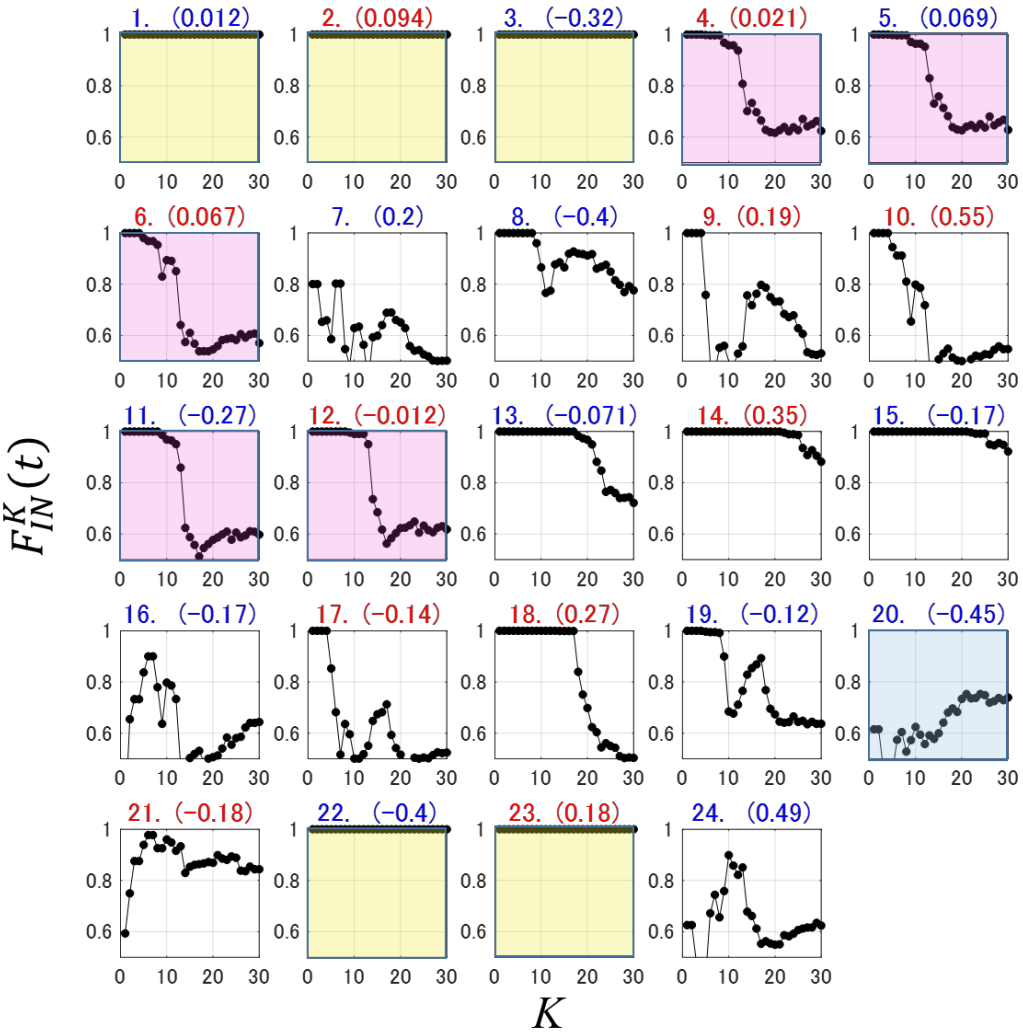

Fig. 5. Spatio-temporal behaviour of the phase synchronisation for the selected period in the case of (e_C, ε, α) = (0.05, 0.2, 0.4) and R_C = 1.4. $F_{IN}^{K}(t)$ vs K plots for t = 1, 2, …, 24; t and the common noise $CE(t)$ are listed at the top of each panel; ON-year and OFF-year are shown in red and blue, respectively.

Notably, perfect in-phase synchronisation occurred even when the external force (common noise) is small. For example, for t = 1 and 2, perfect in-phase synchronisation (mode-locking) occurred, but the external forces were small, with $e_C(1)$ = 0.012 and $e_C(2)$ = 0.094, respectively. Conversely, even when a large external force (common noise) was imposed, almost complete desynchronisation occurred. In fact, no significant phase synchronisation occurred despite the very high external force at t = 24 ($e_C(24)$ = 0.49). These insights were deduced from the developed mathematical model and provide a new perspective on the response of plant populations to environmental inputs.

4. DISCUSSION

Our study suggests that endogenous switching network dynamics and exogenous environmental forces act together to produce the various phase synchronisations seen in alternating bearing and/or masting. Consequently, the following two hypotheses can be derived. The first hypothesis is that the cropping coefficient m increases from west to east due to site-specific factors such as the westerly in California and topographical conditions. The west-to-east increase of synchronisation intensity is a site-dependent feature, which need not appear in orchards with different site conditions.

The second hypothesis is that diffusive coupling by root grafting/mycorrhizal networks exists, which leads to underground interactions between trees [17, 27]. Numerical experiments confirmed that diffusive coupling is essential for the occurrence

of spatial correlation. Since diffusive coupling depends on the development of the root system, the spatial distribution of diffusive coupling should vary among orchards. Future field studies would test these hypotheses.

The proposed methodology based on nonlinear dynamics should be useful for pomology, forestry, and ecosystem management. Suppressing alternating bearing is possible by reducing phase synchronisation. Therefore, if the spatial gradient of the phase synchronisation would occur due to the pollen density, as claimed in Figs. 4a and c, we can moderate alternate bearing by increasing the number of male trees in the targeted area. Furthermore, if the diffusive coupling by root system networks enhances phase synchronisation, disrupting the root system network with a subsoiler or pan breaker may relieve alternate bearing. In addition, the spatial correlation of fruit yield can be a valid indicator to estimate root system development. Thus, revealing the nonlinear dynamics behind perennial plant populations will open new avenues for agricultural management. Furthermore, as noted in subsection *3.1.1 Chaotic Oscillator*, the presence of mathematically equivalent dynamics both in the perennial plant reproduction and in the electronic circuits of booster converters is not a coincidence. This implies that collaboration between nonlinear mathematics and plant science may open new horizons of research.

Acknowledgements

K.S. would like to thank Prof. Eliezer Goldschmid (emeritus professor of agriculture at the Hebrew University of Jerusalem), Prof. Awadesh Prasad (Department of Physics and Astrophysics, University of Delhi), and Prof. Rajarshi Roy (Institute for Research in Electronics and Applied Physics, University of Maryland) for the productive conversations. K.S. would also like to acknowledge JSPS Grants-in-Aid

Nos. 20K21347 and 23380152. A.H. acknowledges NSF DMS – 1840221 NSF DMS – 184022.

Author contributions

K.S., P.B., S.U., and A.H. conceived the research. P.B. and R.T. designed the field survey, performed the measurements, and established the dataset. K.S. conducted the numerical simulations, analysed the results, and prepared the manuscript. All the authors participated in discussions and provided intensive suggestions for improving the manuscript.

Ethics declarations

Competing interests

The authors declare no competing interests.

Research involving plants

All research and experiments conducted during this research are fully compliant with all relevant institutional, national, and international guidelines and legislation.

Data availability

The data are available in the Supplementary Information.

References

[1] Goldschmidt EE. Plant grafting: new mechanisms, evolutionary implications. Front Plant Sci 2014;5:2014.00727. https://doi.org/10.3389/fpls.2014.00727.

[2] Sakai K. Nonlinear dynamics and chaos in agriculture systems. Amsterdam: Elsevier Science; 2001.

[3] Prasad A, Saka K. Understanding the alternate bearing phenomenon: Resource budget model. Chaos 2015;25:123102–6. https://doi.org/10.1063/1.4936673.

[4] Li CY, Weiss D, Goldshmidt EE. Girdling affects carbohydrate- related gene expression in leaves, bark and roots of alternate- bearing citrus trees. Ann Bot 2003;92(1):137–43. https://doi.org/10.1093/aob/mcg108.

[5] Kon TM, Schupp JR. Apple crop load management with special focus on early thinning strategies: a US perspective. Hortic Reviews 2019;46:255–98.

[6] Khalil SK, Mexal J, Khalil IH, Wahab S, Rehman A, Hussain Z, et al. Foliar ethephon fruit thinning improves nut quality and could manage alternate bearing in pecan. Pharm Chem J 2016;3:150–6.

[7] Lyles D, Rosenstock TS, Hastings A, Brown PH. The role of large environmental noise in masting: General model and example from pistachio trees. J Theor Biol 2009;259(4):701–13. https://doi.org/10.1016/j.jtbi.2009.04.015.

[8] Rosenstock TS, Rosa UA, Plant RE, Brown PH. A reevaluation of alternate bearing in pistachio. Sci Hortic 2010;124:149–52. https://doi.org/10.1016/j.scienta.2009.12.007.

[9] Rosenstock TS, Hastings A, Koenig WD, Lyles DJ, Brown PH. Testing Moran' s theorem in an agroecosystem. Oikos 2011;120:1434–40. https://doi.org/10.1111/j.1600-0706.2011.19360.x.

[10] Koenig WD, Knopes JMH. The mystery of masting in trees. Am Sci 2005;93:340–7.

[11] Kelly D, Sork VL. Mast seeding in perennial plants: why, how, where? Annu Rev Ecol Syst 2002;33:427–47. https://doi.org/10.1146/annurev.ecolsys.33.020602.095433.

[12] Satake A, Iwasa Y. Pollen coupling of forest trees: Forming synchronized and periodic reproduction out of chaos. J Theor Biol 2000;203:63–84. https://doi.org/10.1006/jtbi.1999.1066.

[13] Satake A, Iwasa Y. The synchronized and intermittent reproduction of forest trees is mediated by the Moran effect, only in association with pollen coupling. J Ecol 2002;90:830–38. https://doi.org/10.1046/j.1365-2745.2002.00721.x.

[14] Satake A, Iwasa Y. Spatially limited pollen exchange and a long-range synchronisation of trees. Ecology 2002;83:993–1005. https://doi.org/10.1890/0012-9658(2002)083[0993:SLPEAA]2.0.CO;2.

[15] Isagi Y, Sugimura K, Sumida A, Ito H. How does masting happen and synchronize? J Theor Biol 1997;187:231–9. https://doi.org/10.1006/jtbi.1997.0442.

[16] Prasad A, Sakai K, Hoshino Y. Direct coupling: a possible strategy to control fruit production in alternate bearing. Sci Rep 2017;7:39890. https://doi.org/10.1038/srep39890.

[17] Sakai K, Hoshino Y, Prasad A, Fukamachi A, Ishibashi A. Period-3 dominant phase synchronisation of Zelkova serrata: n order-collision bifurcation observed in a plant population. Sci Rep 2019;9:15568. https://doi.org/10.1038/s41598-019-50815-8.

[18] Noble AE, Rosenstock TS, Brown PB, Machta J, Hastings A. Spatial patterns of tree yield explained by endogenous forces through a correspondence between the Ising model and ecology. PNAS 2018;115(8):1825–30. https://doi.org/10.1073/pnas.1618887115.

[19] Akita T, Sakai K, Iwabuchi Y, Hoshino Y, Ye X. Spatial autocorrelation in masting phenomena of Quercus serrata detected by multi-spectral imaging. Ecol Model 2008;215(1–3):217–24. https://doi.org/10.1016/j.ecolmodel.2008.02.029.

490 [20] Crone EE, Rap JM. Resource depletion, pollen coupling, and the ecology of mast
491 seeding. Ann N.Y. Acad Sci 2014;1322:21–34. https://doi.org/10.1111/nyas.12465.
492 [21] Noble AE, Machta J, Hastings A. Emergent long-range synchronisation of
493 oscillating ecological populations without external forcing described by Ising
494 universality. Nat Commun 2015;6:6664. https://doi.org/10.1038/ncomms7664.
495 [22] Kaeko K. Spatiotemporal intermittency in coupled map lattices, Prog Theor
496 Physics 1985;74(5):1033–4044. https://doi.org/10.1143/PTP.74.1033.
497 [23] Kaneko K. Globally coupled chaos violates the law of large numbers but not the
498 central-limit theorem. Phys Rev Lett 1990;65:1391–4.
499 https://doi.org/10.1103/PhysRevLett.65.1391.
500 [24] Zhou C, Kurths J. Noise-induced phase synchronisation and synchronisation
501 transitions in chaotic oscillators. Phys Rev Lett 2002;88:230602.
502 https://doi.org/10.1103/PhysRevLett.88.230602.
503 [25] Pecora LM, Carroll TL. Synchronisation in chaotic systems. Phys Rev Lett
504 1990;64:821–4. https://doi.org/10.1063/1.4917383.
505 [26] Rosenblum MG, Pikovsky AS, Kurths J. Phase synchronization of chaotic
506 oscillators. Phys Rev Lett 1996;76(11):1804–7.
507 https://doi.org/10.1103/PhysRevLett.76.1804.
508 [27] Klein T, Siegwolf RTW, Körner C. Belowground carbon trade among tall trees in a
509 temperate forest. Science 2016;352(6283):342–4.
510 https://doi.org/10.1126/science.aad6188.
511 [28] Graham B, Bormann F. Natural root grafts. Bot Rev 1966;32:255–92.
512 https://doi.org/10.1007/BF02858662.

513 [29] Lev-Yadun S. Why should trees have natural root grafts? Tree Physiol
514 2011;31:575–8. https://doi.org/10.1093/treephys/tpr061.
515 [30] van der Heijden MGA, Klironomos J, Ursic M, Moutoglis P, Streitwolf-Engel R,
516 Boller T, et al. Mycorrhizal fungal diversity determines plant biodiversity, ecosystem
517 variability and productivity. Nature 1998;396:69–72. https://doi.org/10.1038/23932.
518 [31] Simard SW, Pery DA, Jones MD, Myrold DD, Durall DM, Molina R. Net transfer
519 of carbon between ectomycorrhizal tree species in the field. Nature 1997;388:579–82.
520 https://doi.org/10.1038/41557.
521 [32] Gaion LA, Carvalho RF. Long-distance signaling: What grafting has revealed?. J
522 Plant Growth Regul 2018;37:694–704. https://doi.org/10.1007/s00344-017-9759-6.
523 [33] Esmaeili S, Hastings A, Abbott K, Machta J, Nareddy VR. Density dependent
524 Resource Budget Model for alternate bearing. J Theor Biol 2020;509:110498.
525 https://doi.org/10.1016/j.jtbi.2020.110498.
526 [34] Ye X, Sakai K. Limited and time-delayed internal resource allocation generates
527 oscillations and chaos in the dynamics of citrus crops. Chaos 2013;23:043124.
528 https://doi.org/10.1063/1.4832617.
529 [35] Moran PAP. The statistical analysis of the Canadian Lynx cycle. 2. Synchronisation
530 and meteorology. Aust J Zool 1953;1:291–8.
531 [36] Hoch G, Siegwolf RTW, Keel SG, Körner C, Han Q. Fruit production in three
532 masting tree species does not rely on stored carbon reserves. Oecologia 2013;171:653–
533 62. https://doi.org/10.1007/s00442-012-2579-2.
534 [37] Ichie T, Igarashi S, Yoshida S, Kenzo T, Masaki T, Tayasu I. Are stored
535 carbohydrates necessary for seed production in temperate deciduous trees? J Ecol
536 2013;101:525–31. https://doi.org/10.1111/1365-2745.12038.

[38] Banerjee, S., Karthik, M. S., Yuan, G. & Yorke, J. A. Bifurcations in One-Dimensional Piecewise Smooth Maps-Theory and Applications in Switching Circuits. IEEE T Circuits-I 2000;47:389–94. https://doi.org/10.1109/81.841921.

[39] Banerjee, S., Ranjan, P. & Grebogi, C. Bifurcations in Two-Dimensional Piecewise Smooth Maps-Theory and Applications in Switching Circuits. IEEE T Circuits-I 2000;47:633–43 (2000). https://doi.org/10.1109/81.847870.